Korean J. Chem. Eng., **28**(1), 56-63 (2011)
DOI: 10.1007/s11814-010-0327-z

Chaotic behavior of in-line bubbles rising with coalescences in non-Newtonian fluids: A multiscale analysis

Shaokun Jiang*, Youguang Ma*,†, Wenyuan Fan*, Ke Yang*, and Huaizhi Li**

*State Key Laboratory of Chemical Engineering, School of Chemical Engineering and Technology, Tianjin University, Tianjin 300072, China
**Laboratoire des Sciences du Génie Chimique, Nancy-Université, CNRS, 1, rue Grandville, BP 451, 54001 Nancy cedex, France
(*Received 27 February 2010 • accepted 19 May 2010*)

Abstract−The nonlinear dynamics of in-line bubbles rising with coalescence in non-Newtonian Carboxymethylcellulose sodium (CMC) fluids was studied through the techniques such as the multiresolution signal decomposition and the chaotic time series analysis. The temporary signals of bubble passages collected by an optical sensing device at different heights were investigated by a 12-level wavelet decomposition and the scalewise characteristics of bubble motion were extracted and analyzed. The chaotic time series analysis distinguished the periodicity or the deterministic chaos of bubble motion successsfully. The calculation of Kolmogorov entropy proves that in the ranges of experimental heights and gas flowrates, the bubble rising dynamics becomes more chaotic with the increase of height, and reaches the maximum chaotic extent in a certain height, while with the further increase of height, the chaotic extent decreases slowly. With the increase of gas flowrate, at the lower height, the bubble rising dynamics changes from periodicity to deterministic chaos, and at the higher heights it reaches the maximum chaotic extent in a certain gas flowrate; however, for both cases, it has little change in the higher gas flowrates. Moreover, with the increase of CMC concentration, the bubble rising dynamics becomes less chaotic when the height is beyond a certain value.

Key words: Bubble, Coalescence, Wavelet Decomposition, Chaos, Kolmogorov Entropy

INTRODUCTION

Gas-liquid two-phase flows involving non-Newtonian fluids are widely encountered in many industrial processes, such as gas-liquid contact, gas-liquid separation, gas absorption, and bubble column. Bubbles in non-Newtonian fluids display complicated behavior, especially the coalescence between rising bubbles. The interfacial area between phases is reduced and the liquid film at the gas/liquid interface desquamates and renews due to bubble coalescence, leading to a significant impact on mass and heat transfer.

Few studies on bubble coalescence in non-Newtonian fluids have been reported due to its complex nature. The rupture time of the thin film separating two bubbles in non-Newtonian fluids was measured by a high speed camera [1]. The bubble coalescence in viscoelastic fluids was visually observed by injecting two or three bubbles of different volumes [2,3]. Afterwards, Li et al. [4] recorded the frequency signal of bubble passage at different heights in viscoelastic fluids via an optical sensing device, and based on the time delay embedding method of reconstructing the phase-space diagram, the calculated results of the largest Lyapunov exponent, the correlation dimension and the phase portrait revealed that the bubble coalescence in viscoelastic fluids obeys a deterministic and chaotic mechanism. Furthermore, a mathematical model was developed to describe the complex nonlinear dynamics of bubble chains rising in viscoelastic fluids [5]. However, the fundamental mechanism on bubble coalescence in non-Newtonian fluid is still far from fully understood.

In the present work, an optical sensing system was employed to acquire the temporary signals of bubble passages in a non-Newtonian fluid at different heights. Due to the influence of particles in the fluid and the variation of the laser beam itself, the temporary signal of bubble passages, including the information of various motions, was quite complicated and needed to be analyzed using proper and efficient methods to distinguish the dynamics of rising bubbles. Recently, the multiresolution signal decomposition [6] has been widely applied to analyze pressure fluctuation signals with multiscale features and unsteady characteristics in fluidization and bubble columns in chemical engineering [7-12]. Another technique, the chaotic time series analysis, has also shown great advantages in studying the nonlinear dynamics of bubble columns [4,13,14]. In the present work, both the multiresolution signal decomposition and chaotic time series analysis were simultaneously employed to analyze the temporary signals of bubble passages in non-Newtonian fluids and then to characterize qualitatively and quantitatively the nonlinear dynamics of in-line bubbles rising with coalescences.

EXPERIMENTAL

1. Collection of the Temporary Signal of Bubble Passages

The experimental setup is shown in Fig. 1. A Plexiglas square tank with the size of 0.15×0.15×1.50 m was constructed. Nitrogen bubbles were continuously formed through an orifice of a diameter 1×10^{-3} m, submerged in the liquid at the central bottom of the tank

†To whom correspondence should be addressed.
E-mail: ygma@tju.edu.cn

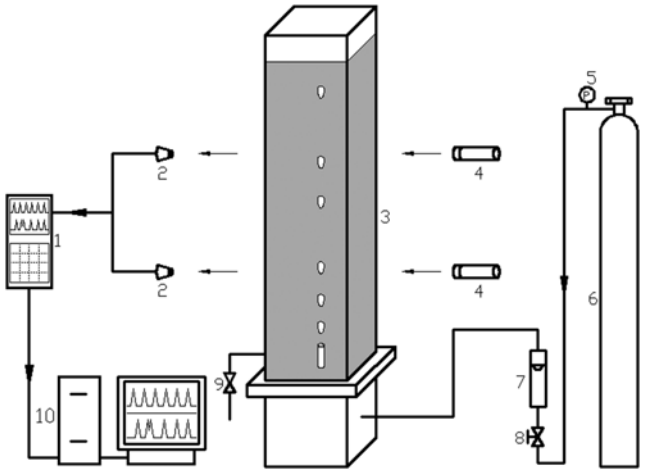

Fig. 1. Schematic diagram of the experimental setup and process.

1. Operational amplifier and sample unit
2. Photodiodes
3. Plexiglas square tank
4. Semiconductor lasers
5. Manometer
6. Compressed nitrogen cylinder
7. Rotameter
8. Pressure maintaining valve
9. Valve
10. Computer

under a constant gas flowrate. A large Plexiglas reservoir was installed right below the tank to avoid the pressure fluctuations due to bubble formation and detachment. An optical sensing system, including double lasers, double photodiodes, an operational amplifier, a sample unit and a computer, was used in collecting the temporary signal of bubble passages. The laser beam irradiated a wall of the tank perpendicularly and passed through the bubbles' rising trajectory. When a bubble rose into the beam, only a part of the light passed through the bubble due to the reflection of the bubble surface, and the variation of the light was detected in form of electric voltage by the photodiode on the other side of the tank. All the experiments were carried out at room temperature.

2. Non-Newtonian fluids

Carboxymethylcellulose sodium (CMC) aqueous solutions of various concentrations 1.0, 1.3 and 1.6% (wt) with a good light transmission were used as non-Newtonian fluids in this work. Their rheological properties were characterized by a DV-III Ultra Programmable Rheometer (Brookfield Engineering Laboratories, Inc., USA). The results showed that all these CMC solutions exhibited a shear-thinning behavior (Fig. 2).

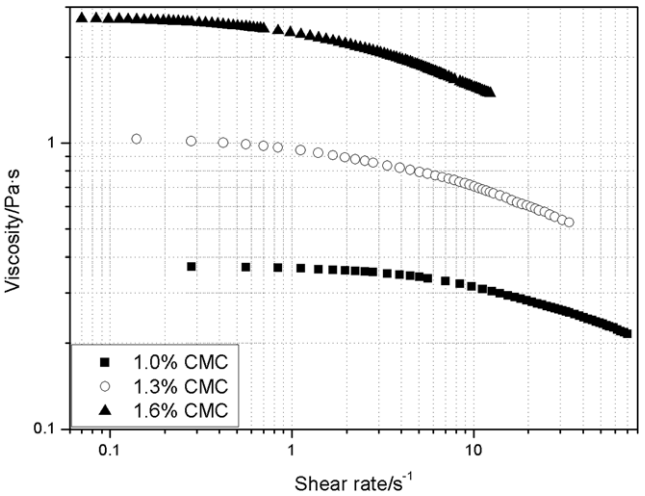

Fig. 2. Variation of viscosity vs. shear rate.

RESULTS AND DISCUSSION

The frequency of bubble formation was acquired from the temporary signal measured near the orifice, and the initial bubble volume at the same height was evaluated by a photograph method. The initial equivalent diameter of bubble was then calculated by the equation, $d_{eq}=(6V_B/\pi)^{1/3}$, in which V_B is the bubble volume. Fig. 3 shows the variations of the frequency of bubble formation and the initial equivalent diameter of bubble *vs.* gas flowrate in the CMC solutions. Besides, bubble rising velocity and bubble size in the range of the whole measured heights were also evaluated by a twin-lased beam system and the photograph method. Under the gas flowrate from 5 to 10×10^{-6} m^3·s^{-1} and the position from 0.1 to 1 m above

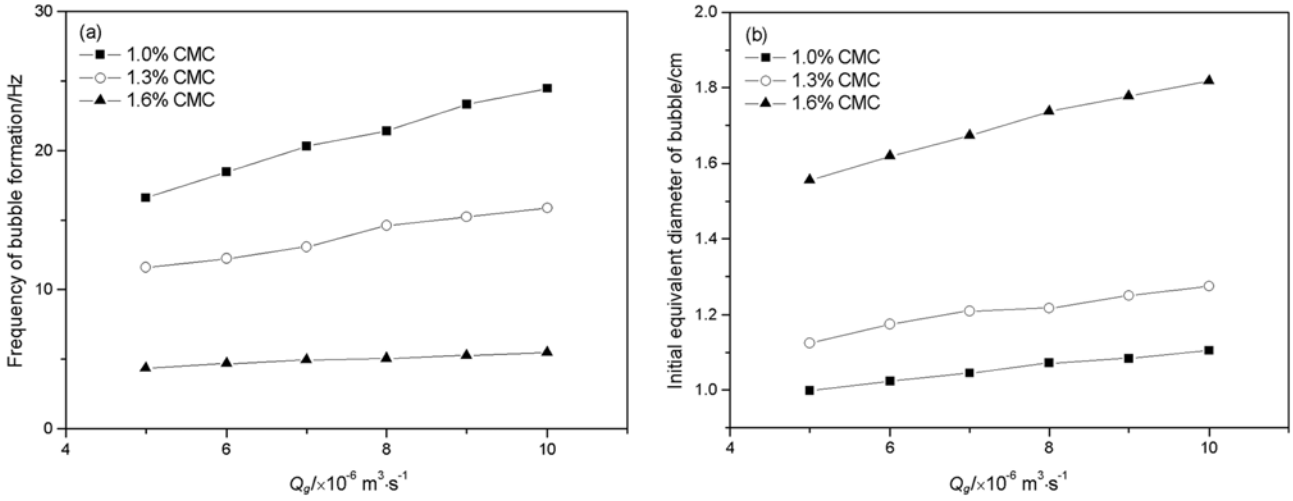

Fig. 3. Variations of the frequency of bubble formation and the initial equivalent diameter of bubble vs. gas flowrate.

the orifice, bubbles' rising velocities varied from 0.20 to 0.40 $m \cdot s^{-1}$, and their volumes from 0.52 to 27.16×10^{-6} m^3. The corresponding Reynolds numbers were between 6.90 and 46.62. Then the shear rate of a rising bubble was estimated as follows [15]:

$$\dot{\gamma} = v/d_{eq} \quad (1)$$

where v is bubble's rising velocity. The shear rate of rising bubbles is between 10.54 and 25 s^{-1} in this work, locating then in the shear-thinning range.

1. Temporary Signal of Bubble Passages

Fig. 4 shows a typical temporary signal of bubble passages, including multiple high-amplitude pulses, each pulse corresponding to the passage of a bubble. The signal appeared periodic near and just above the orifice under the linear interaction between bubbles due to inertial effects as shown in Fig. 4(a). However, with the increasing height, bubble rising velocity was accelerated due to the interactions between bubbles, leading to the increase of the shear rate of bubbles. As shown in Fig. 3, the formation frequency of bubble formation was high, which brought about the small space distance between bubbles. Therefore, the shear-thinning wake flow of a leading bubble gradually influenced the behavior of its close following bubble before the recovery of the local decreased viscosity. In fact, the local viscosity in the wake of a leading bubble was decreased so that the following bubble could rise faster with a reduced drag [4,5]. A PIV measurement revealed that the fluid flow is upward in the wake of a bubble rising in CMC solutions [16], which also promoted its close following bubble accelerating. Under the dual action of the shear-thinning effect and the wake of the leading bubble, the following bubble could catch up with the leading one to produce a coalescence resulting in a big bubble. With the appearance of the coalescence, a bubble chain was then destroyed and the interactions between bubbles became no longer linear. Obviously, the temporary signal of bubble passages appeared irregular with bifurcation pulses indicating the coalescences (Fig. 4(b)).

From the temporary signal of bubble passage, the quantities of bubbles and coalescences can be counted statistically in unit time. The variation of the quantities of bubbles and coalescences in 60 s at certain heights is shown in Fig. 5. With the increase of height, the quantity of bubbles decreases due to the coalescence, and at certain heights, the coalescences are frequent.

2. Multiscale Characteristics

To investigate the rising dynamics of bubbles in CMC solutions from a multiscale view, a multiresolution method, wavelet analysis, was employed in this work. Wavelet transform is a novel signal pro-

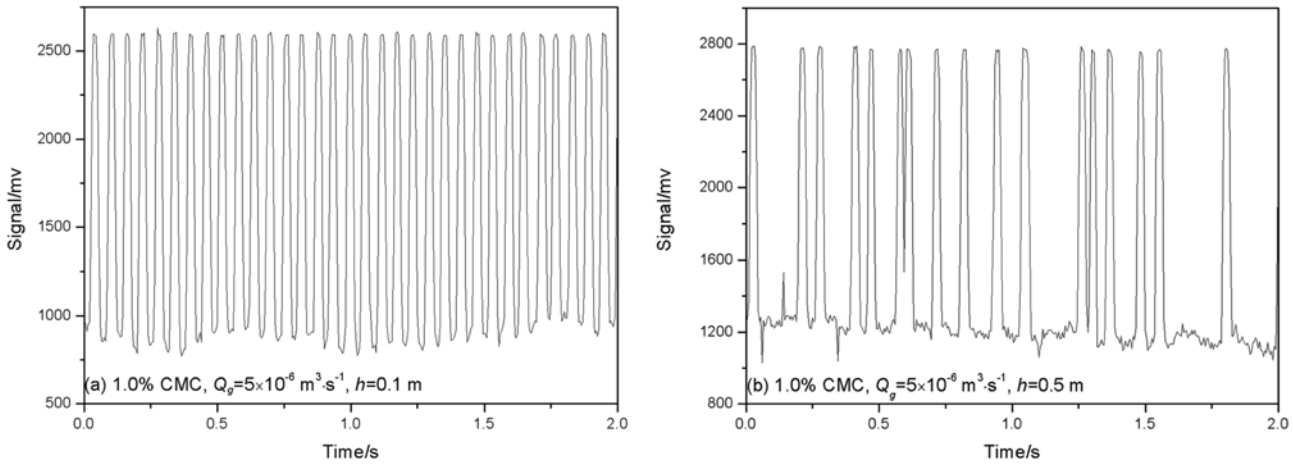

Fig. 4. Typical temporary signal of bubble passages in 1.0% CMC, Q_g=5×10^{-6} $m^3 \cdot s^{-1}$, (a) h=0.1 m; (b) h=0.5 m.

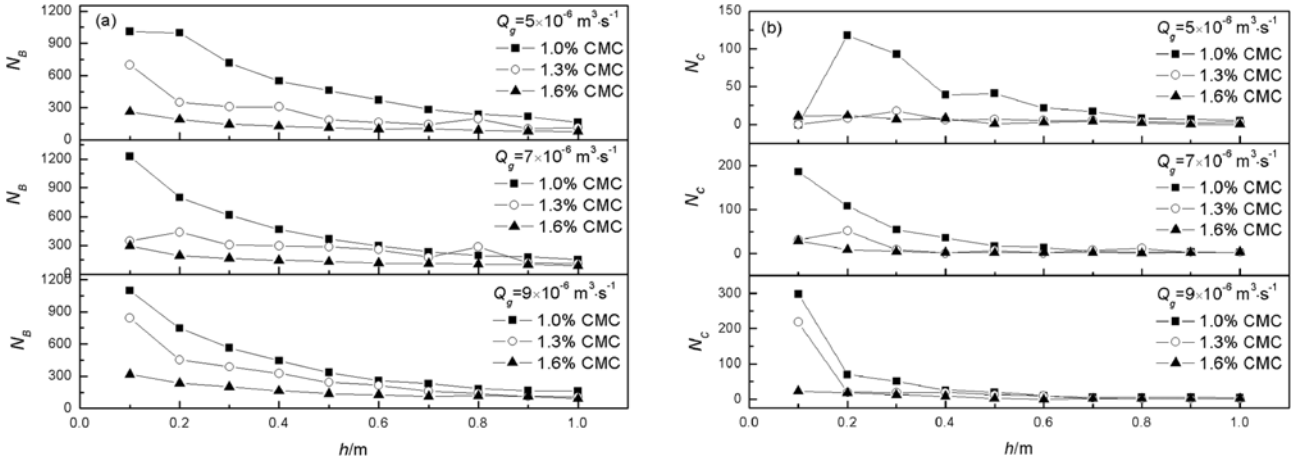

Fig. 5. Variations of bubble quantity and coalescence quantity under different conditions, (a) Bubble quantity; (b) Coalescence quantity.

cessing method. Unlike the windowed Fourier transform, the wavelet transform can provide more flexible time-frequency resolutions on the spectral components. Daubechies wavelet has been widely used due to its simple structure and good repeatability. In this work, Daubechies4 (db4) was selected as the wavelet basis function. The scalewise detail signals were obtained by a 12-level wavelet decomposition.

$$D_i(i) - \sum_k d_{j,k}\psi_{j,k}(i) \quad (2)$$

where detail coefficients $d_{j,k} = \int x(i)\,\psi_{j,k}(i)di$, x(i) is the normalized temporary signal of bubble passages, and base function $\Psi_{j,k}(i)$ obtained through the dilation and translation of the orthogonal wavelet function Ψ.

$$\psi_{j,k}(i) = 2^{-j/2}\,\psi(2^{-1}i - k) \quad j, k \in I \quad (3)$$

where integer j is the level of wavelet transform, varied from 1 to 12, k the time shift, varied as 1, 2, …, $N/2^j$ and N the number of

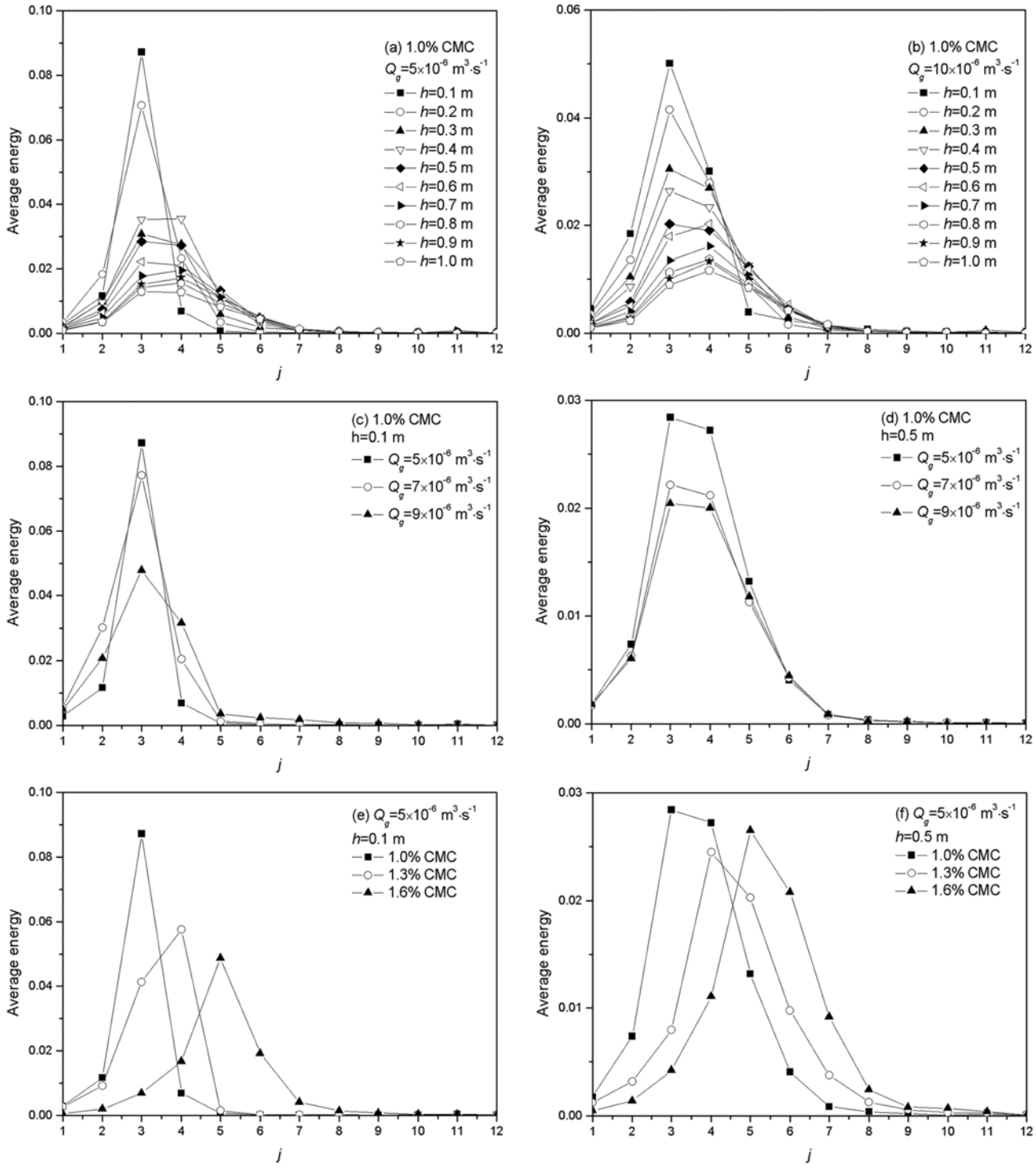

Fig. 6. Scalewise distributions of the average energy obtained with the temporary signals of bubble passages.

data points. At each level j, $D_j(i)$, which reflects the high-frequency features at level j, covers an approximate frequency domain of [$f_s/2^{j+1}$, $f_s/2^j$], where f_s is the sampling frequency.

Then the average energy of different scales could be described as follows:

$$P_j = \frac{1}{N}\sum_{i=1}^{N}|D_j(i)|^2 \quad (4)$$

The scalewise distributions of the average energy obtained with the temporary signals of bubble passages are shown in Fig. 6. As shown in Fig. 6(a) and 6(b), the energy is mainly distributed in the levels j=2-6 and the maximum energy level approximates to 3 or 4. According to the feature of bubble motion, the energy range primarily describes the characteristics of the bubble motion, while the other levels covered lower energy, such as level j=1 represents the random components, and levels j>6 describe some macro motions like particles with fluid. For the case of gas flowrate $Q_g=5\times10^{-6}$ $m^3\cdot s^{-1}$, in the lower position, bubbles still behave periodic rising with single motion frequency, leading to a narrow energy range; however, with the increase of height, as mentioned above, bubble coalescence occurs, which breaks the periodic rising bubble chain and forms irregular motion frequencies of bubbles, resulting in the wider energy range. For the case of $Q_g=10\times10^{-6}$ $m^3\cdot s^{-1}$, in the lower position, the spatial distance of adjacent formatted bubbles decreases due to the increasing frequency of bubble formation under the high gas flowrate (Fig. 3(a)), and bubble interaction strongly affects bubbles rising, leading to the occurrence of coalescence at the lower height; therefore, the regular in-line bubble chain is destroyed and the width of energy range increases. While at the higher height, similar with the case of $Q_g=5\times10^{-6}$ $m^3\cdot s^{-1}$, owing to the irregular motion of bubbles, the wider energy ranges are shown. Fig. 6(c) shows clearly the relation that the energy range becomes wider with the increase of gas flowrate in the lower height; however, at the higher height, as shown in Fig. 6(d), the variation of gas flowrate has little effect on the width of energy range, i.e., the frequency ranges of bubble motion are the same under such conditions. With the increase of CMC concentration, the apparent viscosity of the solution increases, leading to the smaller frequency of bubble formation (Fig. 3(a)), and the formatted bubble size also increases (Fig. 3(b)), making the drag force on the bubble increased to restrain its rising. As a result, the energy range moves towards the large scale area, i.e., the low-frequency domain (Fig. 6(e) and 6(f)).

3. Chaotic Characteristics of Bubble Dynamics

As mentioned above, the multiscale characteristics of average energy of bubbles motion were obtained by the analysis of wavelet decomposition. However, the quantitative features of bubbles dynamics are still unclear. To acquire the interrelated information of bubble motion, the detail signals of the energy range, $x_e(i)$, were extracted and summed to weaken the effect of random components and other motions. Then the time-delay embedding method was employed to reconstruct a phase space:

$$X(i)=[x_e(i), x_e(i+\tau), \ldots, x_e(i+(d-1)\tau] \quad i=1, 2, \ldots, N-(d-1)\tau \quad (5)$$

where τ and d represent, respectively, the time delay and the embedding dimension. The determination of the appropriate value of τ plays a key role in the correct phase space reconstruction. In this work, the multiple autocorrelation method [17], which has been successfully applied in many practical signal processing [18], was used to determine τ.

Consider the trajectory shown by Eq. (5) of a d-dimensional dynamical system on a strange attractor. At an interval of τ, the status of the system is measured. Suppose $P(i_1, i_2, ..., i_d)$ is the joint probability of $X(t=\tau)$ in the box i_1, $X(t=2\tau)$ in the box i_2, ..., $X(t=d\tau)$ in the box i_d. Then Kolmogorov entropy is defined as follows [19]:

$$K=-\lim_{\tau\to0}\lim_{l\to0}\lim_{d\to\infty}\frac{1}{d\tau}\sum_{i_1,i_2,\ldots,i_d}P(i_1,i_2,\ldots,i_d)\log_2P(i_1,i_2,\ldots,i_d)$$

where l is the size of the box i_1, i_2, ..., i_d. And the qth-order Renyi entropy is defined as follows:

$$K_q=-\lim_{\tau\to0}\lim_{l\to0}\lim_{d\to\infty}\frac{1}{d\tau}\frac{1}{q-1}\log_2\sum_{i_1,i_2,\ldots,i_d}P^q(i_1,i_2,\ldots,i_d)$$

In general, the second-order Renyi entropy K_2 is a good evaluation of Kolmogorov entropy.

$$K_2=-\lim_{\tau\to0}\lim_{l\to0}\lim_{d\to\infty}\frac{1}{d\tau}\log_2\sum_{i_1,i_2,\ldots,i_d}P^2(i_1,i_2,\ldots,i_d)$$

For a discrete time series, K_2 has the following relation with the correlation integral when τ is constant.

$$K_2=\lim_{r\to0}\lim_{d\to\infty}\frac{1}{m\tau}\log_2\frac{C_d^2(r)}{C_{d+m}^2(r)} \quad (6)$$

where $C_d^2(r)$ is the correlation integral, and K_2 the second-order Renyi entropy, which can be considered as the evaluation of Kolmogorov entropy.

Kolmogorov entropy is a most important measure to characterize the chaotic motion of system. In general, Kolmogorov entropy equaling 0 means that the motion is regular and it approaching infinite indicates that the motion is stochastic, while it being a limited positive value reflects that the motion is chaotic. The chaotic extent of the motion increases with Kolmogorov entropy, i.e., the system becomes more complex.

By means of the time-delay embedding method, the two-dimensional variation of phase trajectory, x(i) vs. $x(i+\tau)$, was reconstructed. In general, for a stable steady state, a periodic motion and a chaotic motion, the phase portraits are a point, a closed curve and a strange attractor, respectively. Fig. 7 shows the typical phase portraits of in-line rising bubbles at different heights. At the height h=0.1 m above the orifice, the phase portrait shows a simple structure with regular rings, signifying the periodic bubbles rising; however, when bubble coalescence occurs at the higher locations, the phase portrait exhibits complicated characteristics of strange attractor that phase trajectories are confined to a finite space and display distinctly a regular and circular structure, but with obvious features of fold and extension. Normally, each circular trajectory refers to an individual frequency. As the height increases further, the phase portraits also show the characteristics of strange attractor. These results corroborate then the deterministic and chaotic mechanism proposed in previous works for bubbles rising in similar fluids [4,5].

Kolmogorov entropies under different experimental conditions are described in Fig. 8. As shown in Fig. 8(a), Kolmogorov entropies under different gas flowrates increase sharply first, then decrease slowly with the increase of height, which represents that the bubble dynamics is less chaotic at the lower height, while with the increase

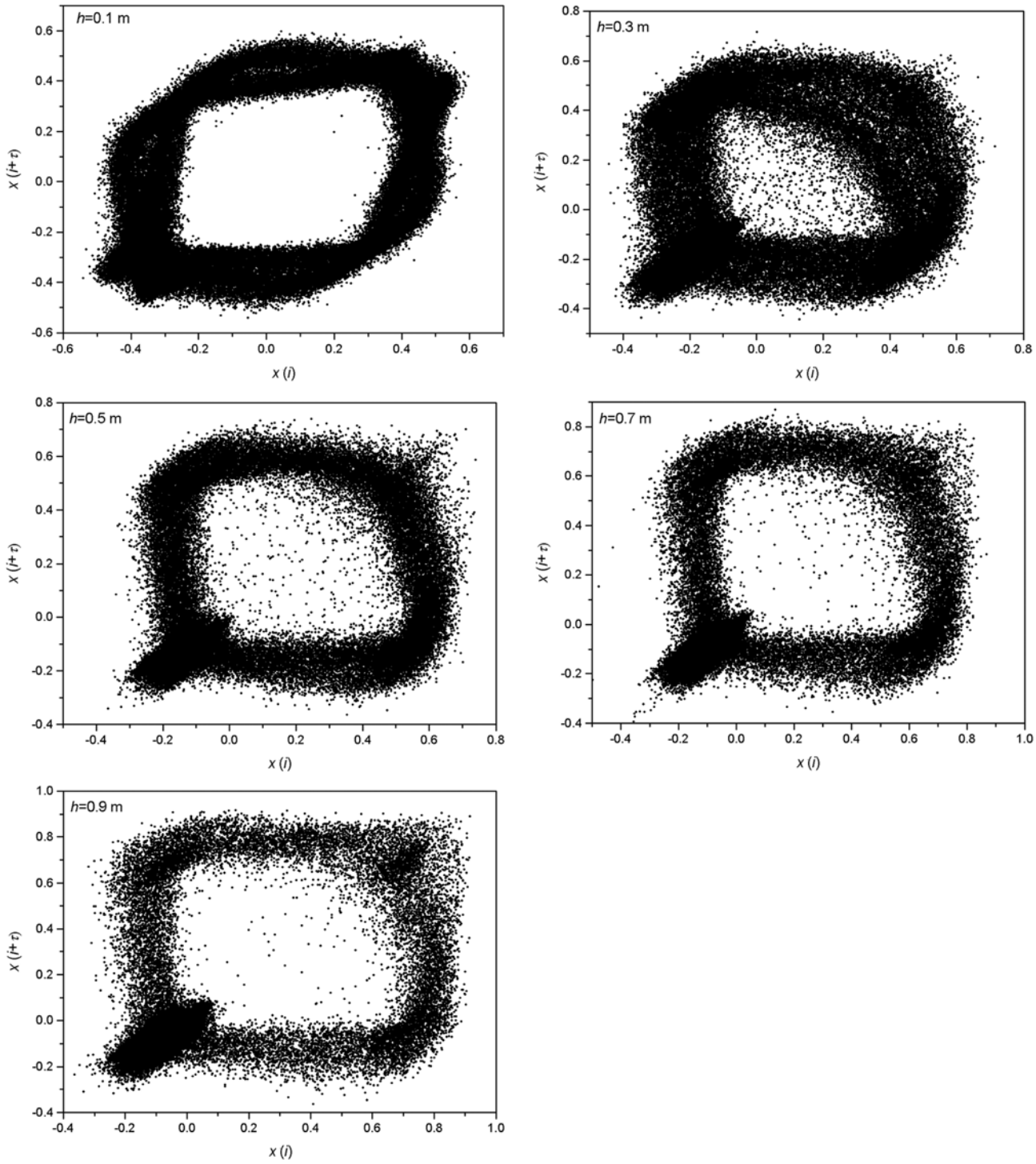

Fig. 7. Phase portraits of in-line rising bubbles at different heights.

of height, the bubble dynamics soon reaches the maximum chaotic extent due to the improved irregularity caused by the frequent bubble coalescences. However, as the height increases further, the chaotic extent is weakened very slowly for the subdued coalescences. Fig. 8(b) displays the variation of Kolmogorov entropy *vs.* gas flowrate. For the case of h=0.1 m, Kolmogorov entropy approximates to 0 when $Q_g=5\times10^{-6}$ $m^3\cdot s^{-1}$ and 6×10^{-6} $m^3\cdot s^{-1}$, symbolizing the periodic bubbles rising. With the increase of gas flowrate, Kolmogorov entropy increases owing to the occurrence of bubble coalescences, reflecting the deterministic chaos of bubbles motion. As the gas flowrate increases further, Kolmogorov entropy has little change, manifesting that the variation of gas flowrate has little effect on the chaotic bubble dynamics. For the cases of h=0.5 m and h=0.9 m, Kolmogorov entropy reaches the maximum value with the maximum chaotic extent when $Q_g=6\times10^{-6}$ $m^3\cdot s^{-1}$, and in the higher gas flowrates, similar with the case of h=0.1 m, the variation of gas

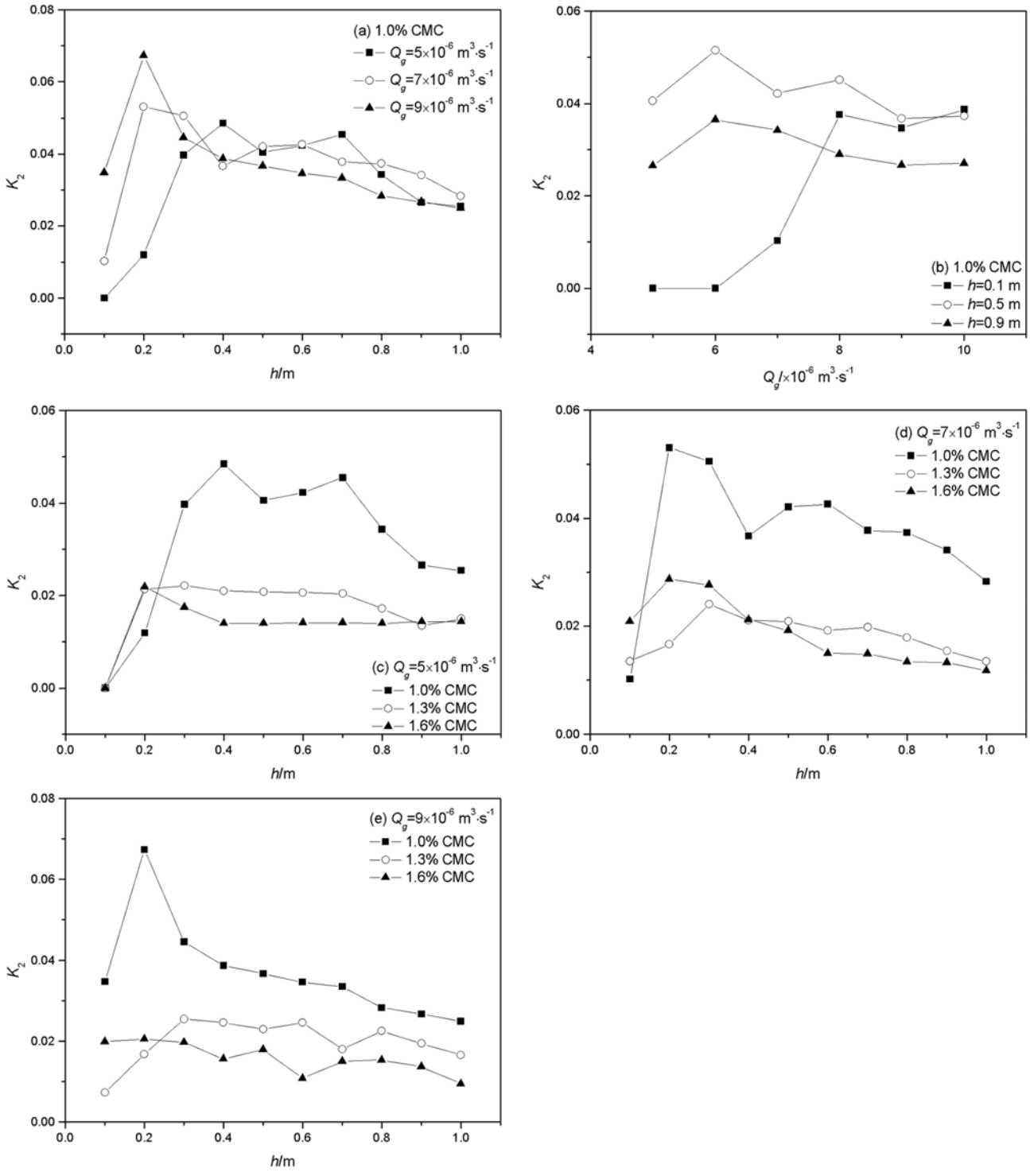

Fig. 8. Variations of Kolmogorov entropy under different conditions.

flowrate also has little influence on the chaotic extent of bubble dynamics for Kolmogorov entropies with little changes. Fig. 8(c)-8(e) show the variation of Kolmogorov entropy *vs.* height in different CMC solutions. With the increase of CMC concentration, as above mentioned, bubble coalescence is restrained; therefore, the irregularity of bubble motion is weakened. When the height is beyond 0.4 m, Kolmogorov entropy decreases with the increase of CMC concentration, reflecting that the chaotic extent of bubble dynamics is weakened with the increase of CMC concentration. However, when the height is less than 0.4 m, the complicated variations of Kolmogorov entropy are shown, which should be caused by the multi action of bubble size, frequency of bubble motion and bubble rising velocity.

The scalewise energy distribution and the quantified chaotic structure throw light on the nature of in-line bubbles rising with coalescence in non-Newtonian fluids. These results could lay the founda-

tion for a better understanding of bubble rising dynamics in such media.

CONCLUSION

The rising dynamics of in-line bubbles rising with coalescence in non-Newtonian fluids was investigated through double approaches: the multiresolution signal decomposition and the chaotic time series analysis.

A 12-level wavelet decomposition reveals the frequency characteristics of bubble motion. The energy range of bubble motion becomes wider with the increase of height for the disturbed frequency of bubble passages led by the bubble coalescence, and at the lower height, the width of the energy range of bubbles motion increases with gas flowrate, while at the higher height, it is barely affected by the variation of gas flowrate. With the increase of CMC concentration, the energy range of bubbles motion moves towards the large scale area, i.e., the primary frequency of bubbles motion decreases.

Based on the chaotic time series analysis, the periodicity and the chaotic structure of bubbles motion were determined. The calculation of Kolmogorov entropy gives the results that owing to the improved irregularity of bubble passages caused by the frequent bubble coalescence, the chaotic extent of bubble rising dynamics increases with height, and attains the maximum value in a certain height, then decreases slowly with the further increase of height due to the weakened irregularity. With the increase of gas flowrate, at the lower height, a dynamical conversion from periodicity to deterministic chaos is shown, while at the higher heights, a maximum chaotic extent is achieved in a certain gas flowrate, and in both cases, bubble rising dynamics has little variations in the higher gas flowrates. With the increase of CMC concentration, the chaotic extent of bubbles rising dynamics decreases when the height is larger than a certain value.

ACKNOWLEDGEMENT

We acknowledge the financial support from the National Natural Science Foundation of China (Grant no. 20476073), Opening Project of State Key Laboratory of Chemical Engineering (No. SKLChE-08B03) and the Programme of Introducing Talents of Discipline to Universities (Grant no. B06006).

NOMENCLATURE

$C_d^2(r)$: correlation integral
d : embedding dimension
d_{eq} : equivalent diameter of bubble [m]
$d_{j,k}$: detail coefficients
D_j : detail signal
h : height above the orifice [m]
j : level of wavelet transform
k : time shift
K_2 : second-order Renyi entropy
m : step increment of embedding dimension
N : number of data points
N_B : quantity of bubbles
N_C : quantity of coalescences
P : average energy
Q_g : gas flowrate [$m^3 \cdot s^{-1}$]
v : bubble's rising velocity [$m \cdot s^{-1}$]
V_B : bubble volume [m^3]
x : normalized temporary signal of bubble passages
x_e : signal extracted from energy range
X : reconstructed phase space

Greek Letters

$\dot{\gamma}$: shear rate [s^{-1}]
τ : time delay
Ψ : orthogonal wavelet function
$\Psi_{j,k}$: base function

REFERENCES

1. A. Acharya and J. Ulbrecht, *AIChE J.*, **24**, 348 (2000).
2. D. De Kee, P. J. Carreau and J. Mordarski, *Chem. Eng. Sci.*, **41**, 2273 (1986).
3. D. De Kee, R. P. Chhabra and A. Dajan, *J. Non-Newtonian Fluid Mech.*, **37**, 1 (1990).
4. H. Z. Li, Y. Mouline, L. Choplin and N. Midoux, *Int. J. Multiphase Flow*, **23**, 713 (1997).
5. H. Z. Li, X. Frank, D. Funfschilling and P. Diard, *Phys. Lett. A.*, **325**, 43 (2004).
6. S. Mallat, *IEEE Trans. Pattern Anal. Mach. Intell.*, **11**, 674 (1989).
7. B. R. Bakshi, H. Zhong, P. Jiang and L. S. Fan, *Trans. IChE*, **73a**, 608 (1995).
8. X. S. Lu and H. Z. Li, *Chem. Eng. J.*, **75**, 113 (1999).
9. J. H. Li, *Power Technol.*, **111**, 50 (2000).
10. H. S. Zhou, J. D. Liu and L. Lin, *Chem. Eng. Sci.*, **55**, 839 (2000).
11. J. Q. Ren, Q. M. Mao, J. H. Li and W. G. Lin, *Chem. Eng. Sci.*, **56**, 981 (2001).
12. W. Nam and G. Y. Han, *Korean J. Chem. Eng.*, **22**, 964 (2005).
13. S. H. Kang, S. M. Son, Y. Kang, J. W. Bae and K. W. Jun, *Korean J. Chem. Eng.*, **25**, 897 (2008).
14. A. Ajbar, W. Al-Masry and E. Ali, *Chem. Eng. Process.*, **48**, 101 (2009).
15. M. Coutanceau and M. Hajjam, *Appl. Sci. Res.*, **38**, 199 (1982).
16. D. Funfschilling and H. Z. Li, *Chem. Eng. Res. Des.*, **84**, 875 (2006).
17. H. G. Ma and C. Z. Han, *Front. Electr. Electron. Eng. China*, **1**, 111 (2006).
18. H. G. Ma and C. Z. Han, *J. Electron.*, **22**, 605 (2005).
19. P. Grassberger and I. Procaccia, *Phys. Rev. Lett.*, **50**, 346 (1983).